Composites Part B 281 (2024) 111533

Contents lists available at ScienceDirect

Composites Part B

journal homepage: www.elsevier.com/locate/compositesb

Analysis of subsurface damage during milling of CFRP due to spatial fibre cutting angle, tool geometry and cutting parameters

Felicitas Böhland [a,*], Andreas Hilligardt [b], Volker Schulze [a]

[a] Institute of Production Science (wbk), Karlsruher Institute of Technolgoy, Kaiserstraße 12, 76131, Karlsruhe, Germany
[b] Reishauer AG, Industriestr. 36, 8304, Wallisellen, Switzerland

ARTICLE INFO

Handling editor: Ole Thomsen

Keywords:
CFRP
Surface analysis
Milling
Fibre cutting angle

ABSTRACT

During machining of carbon fibre reinforced plastics the anisotropy of the material and the resulting cutting conditions can cause various types of damage such as delamination, burrs or subsurface damage. Subsurface damage can lead to a reduction in surface quality or component rejection. In this paper, a new method is used to detect subsurface damage caused by peripheral milling over the entire cut. This analysis, using a newly defined spatial fibre cutting angle θ_{ne}, tool geometry and process parameter, provides a deeper understanding of the damage formation. While the damage area varies with the uncut chip thickness and the rake angle of the tool, the cutting edge rounding and the fibre cutting angle prove to be important in determining the depth of damage. The detected damage area is 44–65 % of the fibre cutting angle range from 0° to 90°, which can be extended up to 12 % due to the damage depth when milling an external radius.

1. Introduction

Due to their beneficial properties such as high strength-to-weight ratio and corrosion resistance, carbon fibre reinforced plastics (CFRP) are particularly used for constantly expanding applications in the aerospace, automotive and wind power industry [1]. The components are manufactured near-net-shape, but in order to meet the high-quality requirements of joining and functional surfaces with sufficient accuracy conventional machining operations are required [2]. However, drilling and milling of CFRP's is still challenging due to the strong material anisotropy and high tool wear rates. The challenging cutting conditions results in various damage defects [3] including delamination [4], burrs [5] and subsurface damages [6]. The damage should be avoided as it leads to cost-consuming post processing, rejection of the whole part or reduced component performance.

The fibre direction is a critical factor as it affects the cutting conditions and influences the occurring damage formation mechanism [7]. A fibre cutting angle is therefore defined, which changes due to the rotational movement of the cutting edge in milling. Different definitions of the fibre cutting angle can be found in literature. Often it is determined two-dimensionally and defined as angle between the cutting direction vector and the unseparated fibre in mathematically positive direction [8]. In orthogonal cutting which is used in many studies to examine the mechanisms the two-dimensional view this is sufficient. There are initial approaches needed for spatial engagement conditions caused by inclination angles, helix angle of the tool or conical tool shapes [9]. In the study by Hintze and Brügmann [9], the effect of the spatial tool inclination on delamination was analysed. There was no cutting angle, but two fibre cutting vectors that separately consider the geometric and kinematic situation relative to the fibre. This makes the analysis detailed, as the effect of 6 factors on damage must be taken into account and the analysis is not based on coherent cutting mechanism. The approach of Zang et al. [10] examines the spatial effect of inclination on burr formation. They take into account the 3D situation due to the change in cutting speed direction. Therefore, it is not possible to transfer and capture changed fibre cutting angles due to twisted tools. Seeholzer et al. [11] take into account the change in the fibre cutting angle through drilling due to changed cutting velocities along the cutting edge, but the cutting angle is still only evaluated in the 2D fibre plane. This does not capture a real spatial fibre cutting angle transferable to different spatial engagement conditions as required for twisted tools.

The different cutting angles of the fibres lead to different failure modes of the material and resulting surface morphologies [3]. The effective separation mechanisms are mostly analysed in the orthogonal cut. In the composite, the load of the cutting edge results in different stresses that can cause complex failure mechanism such as fractures and

* Corresponding author.
E-mail address: felicitas.boehland@kit.edu (F. Böhland).

https://doi.org/10.1016/j.compositesb.2024.111533
Received 8 March 2024; Received in revised form 24 April 2024; Accepted 2 May 2024
Available online 7 May 2024

cracks as well as different fracture surfaces of the fibres [7]. If the fibre is inclined away from the cutting edge (Fig. 1b), local pressure peaks transverse to the fibre lead to breakage [3]. Classically defined this would be the fiber cutting angle range from 90° to 180° referred as along fiber cutting angle (Fig. 1b). Hintze et al. [12] found that this area is the critical fibre cutting angle range in which delamination and burrs at the top layers during slot milling of unidirectional CFRP occurs. In this range the surface roughness is significantly lower [13]. Many researches focus on this area and the resulting delamination damage. In the other area from 0° to 90° degree fibre cutting angles with an inclination of the fibre towards the cutting edge (Fig. 1a), an increased bending load is exerted on the material, which leads to interfacial failure [3]. A different type of damage is predominant in this area called subsurface damage [14]. Surface cavities, saw-tooth profiles and interlaminar cracks are expressions of subsurface damage (see Fig. 1a) and can be caused by the following phenomena: Due to the high bending load, a strong deformation is triggered, which results in fibre-matrix debonding along the fibre orientation. In combination with a compressive bending load, this leads to a shear load on the cutting edge. The cracks spread in advance towards the cutting edge [15]. This often results in a so-called saw tooth profile on the surface observed by Heinrichs et al. [16] among others. Voss [17] detects the influence of the chip thickness and the rake angle on that saw tooth profile in orthogonal turning. This profile becomes larger with greater chip thickness and larger rake angle. Wang et al. [18] investigated the occurrence and formation mechanism of the surface cavity defects. The area of subsurface damage was limited to 50–60 % of the against fibre cutting region, where the roughness was up to 29 % higher than in the along fibre cutting region. In their work changing the process parameters of feed rate and cutting speed had little effect on the damage area. The subsurface damage can lead to complete failure of the CFRP laminate [19]. Modelling approaches show that the tool geometry has a significant influence on the damage depth in along the fibre cutting region [20,21].

In addition to the fibre cutting angle, as in other machining processes, the tool geometry and the process parameters also influence the damage mechanisms during machining process. In Sauer et al. [22] the influence of cutting edge radii during orthogonal cutting was examined. A higher saw tooth profile was observed with larger cutting edge radius. In the against fibre cutting region a larger cutting edge radius leads to more damage in form of delamination and burrs [23]. Due to the cutting edge rounding, the effective rake angle changes, especially with small chip thicknesses, which can have influence on the cutting mechanisms [24]. Often the sharpest possible cutting edge is recommended to avoid delamination, but in industrial practice this results in parts being set until the rounding has reached constant state.

To summarise, previous work has mainly concentrated on delamination and burrs in the upper layers of the workpiece [25]. The rarely investigated interlaminar damage area (subsurface damage) is important for surface quality and possible subsequent bonding [26] and has not yet been sufficiently investigated. Up to now, the investigations have mostly been carried out in orthogonal cutting. However, since milling involves highly complex cutting mechanisms due to continuously changing fibre cutting angles and varying chip thicknesses during tool rotation, it is not possible to completely convert them into quasi-stationary 2D cutting conditions. Previously used spatial fibre cutting angles are not based on the observable directions of the subsurface damage. Therefore in this work, an analysis of the local effects during complete cuts and the application of a spatially defined fibre cutting angle is carried out which refers to division of the effective speed in normal and sliding component of the cutting edge. This will provide deeper insights into the influence on the separation mechanism and the occurrence of the subsurface damage area.

2. Material, tool and experimental setup

The edge trimming of unidirectional carbon fibre reinforced specimens with a material thickness of 6 mm and varying fibre orientations is examined. The processed material is a unidirectional carbon fibre reinforced plastic (UD-CFRP) consisting of an epoxy matrix (CP003) and high tenancy fibres (AS4). The fibre volume content is 60 % and the average fibre diameter is 7 µm. The fibre direction is defined via the global fibre orientation angle Φ (Fig. 2b). The fibre orientations shown in Table 2 are used to obtain different cutting angles during the cut and varying corresponding chip thicknesses. During the investigations, all tests are carried out using tools with a single cutting edge and a diameter of 12 mm. First, a precut is carried out to ensure a constant material allowance towards the following measuring cut. The cutting parameters for the precut are a cutting speed v_c of 100 m/min, a feed per tooth f_z of 0.125 mm and a radial depth of cut a_e of 0.2 mm. In the measurement cut a rapid traverse movement 135° to the feed direction takes place before the milling tool has reached the end, see Fig. 2b. This means that the surface of the last cut is retained and can therefore be analysed further. It becomes apparent what happened over one single milling cut. All the dry peripheral milling tests are performed on a Heller MC16 machining centre.

Force measurement during the process is done by a three component dynamometer (Kistler Type 9255C). The signals are sampled with 10 kHz and a low-pass filter with 3 kHz is applied to reduce signal noise. To reduce the entry frequency, tools with one cutting edge are used and 50 m/min was selected as the cutting speed for the measuring cut, to operate completely below all machine eigenfrequencies. Various tool geometries are used (see Table 1). Despite T2 all cutters are made of

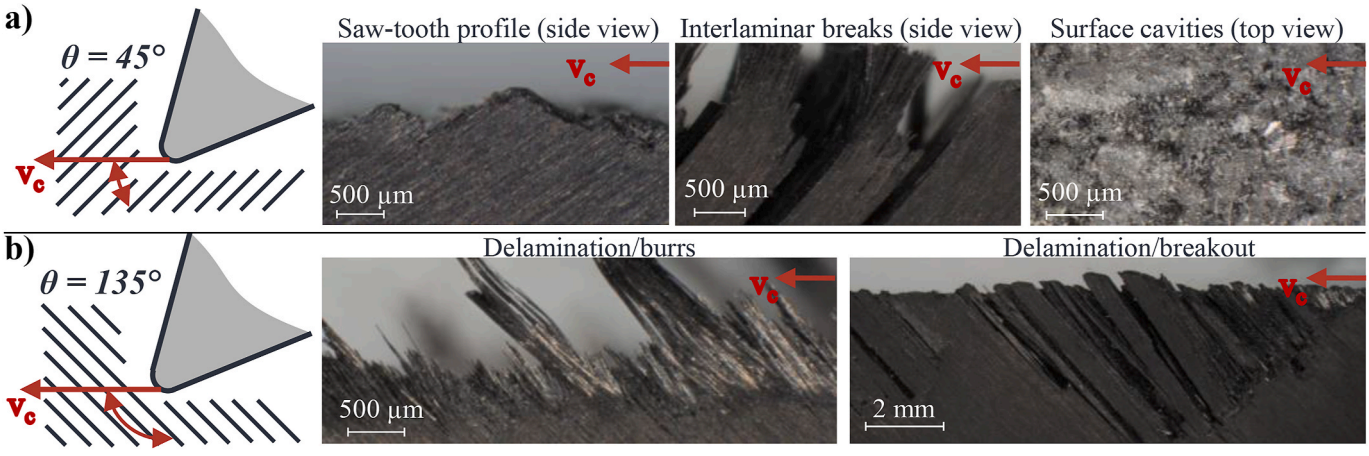

Fig. 1. Schematic illustration of fibre cutting angle where a) mechanism in which surface cavities and b) mechanism in which delamination and burrs occur according to [7].

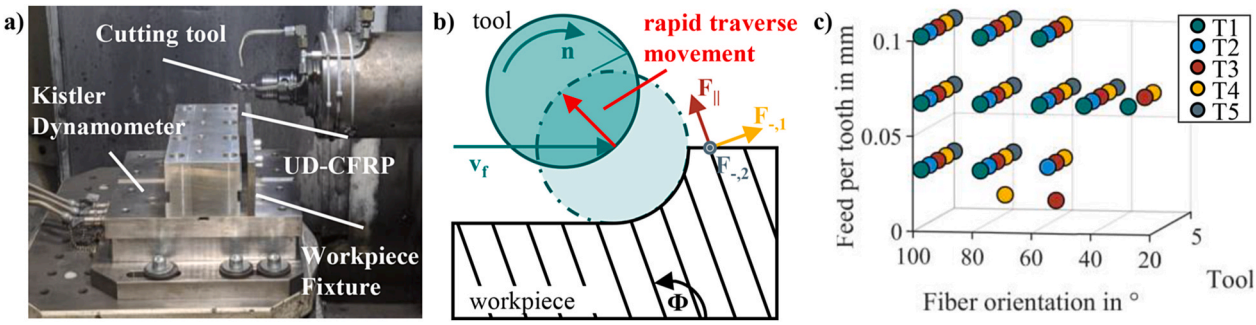

Fig. 2. Experimental procedure with a) the experimental setup in Heller MC 16 machining centre, b) the milling path and c) the experimental design.

Table 1
Tool parameter.

	Ø in mm	Helix angle λ in °	Rake angle γ in °	Clearance angle α in °
T1	12	0°	8°	10°
T2	12	2°	0°	5°
T3	12	30°	25°	15°
T4	12	30°	9°	10°
T5	12	30°	−7°	10°

Table 2
Process parameter.

Milling type	Down milling
Cutting speed v_c in m/min	50
Feed per tooth f_z in mm/tooth	0.01, 0.03, 0.065, 0.1
Radial depth of cut a_e in mm	5.9
Fiber orientation Φ in °	30, 45, 60, 80, 100

cemented carbide and are uncoated. T2 is a polycrystalline diamond (PCD) tool. Rake and clearance angles are defined in the axial section.

The feed rates were selected so that they are within the range recommended by the tool manufacturer and still have a high distance to each other. All experiments are carried out in down milling and with a radial depth of cut of 5.9 mm, which corresponds to almost half the tool radius. The high radial depth of cut a_e was chosen because it allows a wide range of fibre cutting angles to be analysed over a single cut. At the same time it is an advantage that twisted tools remain engaged for a longer time over the entire tool height. Each parameter set is repeated at least twice, while the statistical validation at the experimental parameter set with tool T4, fibre orientation 80° and a feed rate of 0.065 mm/tooth was carried out by a tenfold repetition. The statistical standard deviation for the start and end times detected in the following is 1.05° and 2.56°. The experimental design is shown in Fig. 2c. While the tests were carried out at a feed rate of 0.065 mm/tooth for all milling cutters at Φ from 45° to 100°, the three mainly examined feed rates from 0.03, 0.065 and 0.1 mm/tooth were carried out for the fibre orientations 80° and 100°. The feed rate of 0.01 mm/tooth is outside the tools manufacture's guide values, but was tested for two tools to demonstrate and approve the effects of small chip thicknesses. The fibre orientation of 45° is frequently used industrially, often described as particular damaging and therefore selected. The fibre orientation of 80° is interesting due to the subsurface damage in the centre of the cut without or less damage at the final resulting surface. The other fibre orientations was selected around that two and results in two steps with 20° difference and two with 15°. Fibre orientation 30° and 60° were partially factorial analysed.

3. Evaluation methods

A dexel based geometric penetration simulation is used to calculate local cutting parameters. A two- and a three-dimensional approach were used. While the two-dimensional approach requires minimal computational effort, it is limited to cylindrical tools and processes kinematics without inclinations. The 3D penetration calculation enables the application to more complex tools such as a conical shape and 5-axis kinematics. In the simulation for each discrete kinematic position (rotation angle of the tool), the penetration of the workpiece by the tool along the tool contour normals and thus the local chip thickness according to ISO 3002–1:1982-08 of the unformed chip can be calculated. The vectorial decomposition of the effective speed using the local tool tangent results in the lateral and normal effective speed of the tool according to ISO 3002–1:1982–08, which are also colloquially referred to as sliding and cutting speed. Further detailed information of the simulation can be seen in Hilligardt et al. [27]. The effective fibre normal angle and fibre side angle were introduced for the three-dimensional characterization of the local cutting condition in relation to the fiber orientation. Fig. 3 shows the definition in the free oblique cut. Here, the sign convention and introduction of effective normal fiber cutting angle is analogous to the normal rake angle γ_{ne}, see Fig. 3b. This enables a clear description of the local fiber orientation relative to the cutting edge and tool functional surfaces with reference to the normal speed. Therefore the focus in this work is on the normal fiber cutting angle θ_{ne}. Fig. 4 shows this fibre cutting angle via the rotation angle of the tool without and with helix angle. Due to the simulation it is clear that different fibre cutting angles are engaged at the same time for a twisted tool. Here it comes apparent that the cutting edge points over tool height enter the material one after the other from the first (S_{first}) to the last (S_{last}) cutting edge point.

To enable an evaluation of the surface values and the force measurements with regard to the local cutting parameters, in particular the normal fibre cutting angle θ_{ne}, both the force and the surface measurements are coupled with the simulation. Therefore the force signal of an average cut can be evaluated as time synchronous average for every sample. For this purpose, 80 % of the total signal is used, in particular to exclude transient phenomena when entering the sample. Additionally, local measurement errors are eliminated. In some cases individual sections within the area are analysed, as differences in subsequent cuts become visible and local force peaks can be evaluated. The measured forces are analysed in the workpiece system and the resulting force is divided into forces transverse and parallel to the fibre. The force parallel to the fibre ($F_{\parallel}$) is defined along the fibre orientation and the positive direction points away from the final workpiece surface (Fig. 2b). The first transverse force direction is in the laminate plane ($F_{,1}$) while the second transverse force ($F_{,2}$) is orthogonal to the laminate plane.

A MarSurf XCR 20 roughness and contour measuring device is used to measure the surfaces via tactile profile method. The measurements are taken at a measuring distance of 1 µm and a measuring speed of 0.2 mm/s 50 lines are measured parallel to the feed direction and 0.2 mm to both outer edges of the specimen is maintained. Fig. 5a shows a microscope image of the surface over one cut, in which the structure of the subsurface damage phenomenon can be recognized. The profile lines recorded with the Perthometer are shown schematically in yellow. To evaluate roughness each extracted profile is fitted by the nominal shape

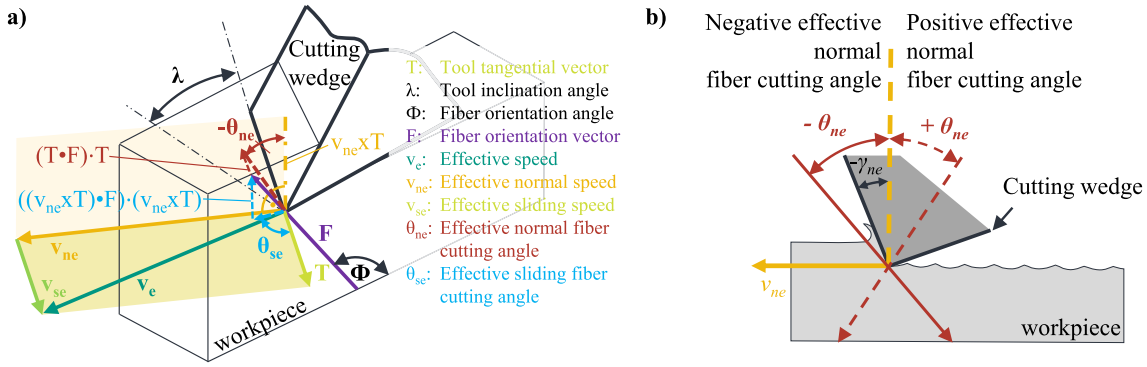

Fig. 3. Fibre cutting angle in a) free oblique cut and in b) effective normal plane.

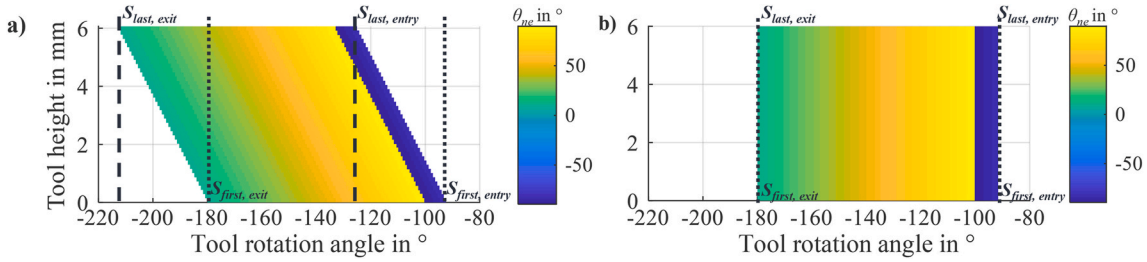

Fig. 4. Fibre cutting angle θ_{ne} via tool rotation and height a) with helix angle and b) without helix angle.

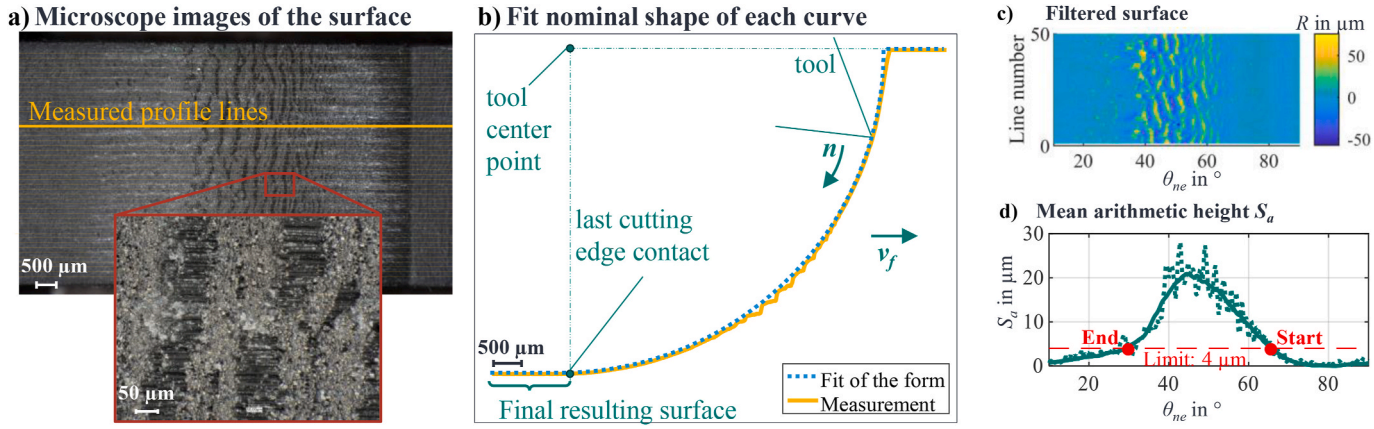

Fig. 5. Surface analysis using tactile profile measurement method.

of the specimen to remove the form, see Fig. 5b. The fit is performed using the MATLAB integrated non-linear least-square optimization. This method also allows to determine the point of the last cutting edge contact and thus the last point of the cut that also lies on the final resulting surface, see Fig. 5b. This point is the centre of the tool in the *x*-direction during the last cut and thus the end of the angles that are passed during one cut. Starting from the tool centre point of the last cut, a straight line is defined to each measurement point, which also intersects the ideal profile. The length between the two intersection points indicated the extent of deviation that can be assigned to an exact angle. This is important in order to assign the fibre cutting angles to the surface roughness by linking them to the simulation of each test point. Subsequent, according to ISO 3274: 1996–12 a low-pass filter with λ_s cut-off of 8 µm is used to remove the micro-roughness and a high-pass filter with λ_c cut-off of 2.5 mm is applied to remove the waviness of each measurement line. The obtained roughness profiles (R) of each of the 50 lines are represented in Fig. 5c. To get an area value, the angles associated with the roughness values of each line are rounded to one decimal place. For all equal angles, the surface roughness parameter mean arithmetic height S_a (Fig. 5d) and maximal height S_z are evaluated in accordance with ISO 25187–2:2021–12. The S_a obtained enables the definition of the subsurface damage area via a limit value. Due to the fact that the maximum acceptable roughness in the industry is around R_a=3.2 µm [28] and the comparison of several measurements the limit value of S_a was set to 4 µm. The intersection points of the limit value with the averaged S_a curve is used to determine the start and end value of the subsurface damage area (Fig. 5d). In addition four samples were measured with the Zeiss metronom 800 C T device to confirm the depth of damage. The voltage for the measurement was 130 kV while for the current 123 µA was selected.

Furthermore the structure of the machined surface is analysed by microscope images with Keyence VHX-7000. The same microscope was used to observe the wear of the cutting edge in fixed intervals. For the test points between the measurements, a linear wear over the cutting path of the cutting edge is interpolated for simplification. The wear was characterized by the cutting-edge rounding r_β.

4. Results and discussions

4.1. Effect of the spatial situation

To capture the 3D cutting situation, the effective normal fibre cutting angle θ_{ne} was introduced (see, Fig. 3b). The results show that due to the defined angle the shift of the subsurface damage area depending on the helix angle can be explained by the spatial definition of the fibre cutting angle (Fig. 6). The comparison of T1 without helix angle and T4 with helix angle of 30° is possible because they have almost the same rake and clearance angle. Fig. 6a shows an offset between the subsurface areas of T1 and T4 in the rotation angle of the tool, which can be converted into the 2D fibre cutting angle used in previous studies. The application of the new definition of the fibre cutting angle shows that the surface damage is in almost the same θ_{ne} range (Fig. 6b). The average angle difference of the start and end θ_{ne} values changes from 6.1° to 2.6°.

The view of the structure across one cut shows the area in which the surface cavity formation mechanism defined by Wang [18] occurs. Comparing the tool T1 without helix angle and T4 with a helix angle, it comes apparent that the structure follows the direction of the effective normal speed v_{ne} (Fig. 3b). Therefore, the structure of the specimens done with twisted tools tilts around the helix angle (Fig. 6). Although the damage structure forms along the helix angle, the start and end of the damage area is a straight line orthogonal to the feed direction. This is evident even though the cutting edge at a defined angle of tool rotation is located at different local fibre cutting angles θ_{ne} and chip thicknesses over the tool height (Fig. 4). This indicates that the geometric conditions define the start and the end of the subsurface damage area and not the engagement situation with different parameters relating to the height of the tool.

4.2. Occurrence and shift factors of the subsurface damage area

4.2.1. Influence of chip thickness on damage area

Fig. 7 show the detected start and end θ_{ne} values of the subsurface damage area plotted against the chip thickness. If no error bars are inserted, the standard deviation is smaller than the symbol. The dashed lines represent the relationship between fibre cutting angle and the uncut chip thickness for one cut and connect corresponding start and end of the damage area. Fig. 7a shows this chip thickness progression over θ_{ne} marked thick for the experiments with $\Phi = 80°$ with 0.065 and 0.03 mm/tooth and $\Phi = 60°$ with 0.065 mm/tooth. A reduction in feed rate and fibre orientation lead to smaller chip thicknesses. However the progression of each curve still differs. For the fibre orientation of 100° for some tools only an end could be detected and for fibre orientation 45° only a beginning. This means that the area begins right at or before the cutting edge enters the specimen material or the area begins just before the cut ends.

The detected damage area is shifted both by changing the feed rate and by changing the fibre orientation. The deviation can be attributed to the influence of the chip thickness. In general, the greater the chip thickness, the earlier the damage area begins. This means that θ_{ne} for the start assumes a higher value for larger chip thickness until a chip thickness less than 0.02 mm. At 0.02 mm and below, a higher deviation in detected start and end values can be determined for most tools from both the same and different trials with similar chip thickness. For T3 with a helix angle of 30° and maximum rake angle of 25° (Fig. 7c) it is apparent that θ_{ne} increases after 0.02 mm with declining chip thickness. This leads to a further increase of the subsurface damage area. From small thicknesses, the importance of the cutting edge rounding becomes proportionally more significant, which explains the change in the trend.

It can be concluded, that the lower the feed rate for samples with the same fibre orientation, the later the area begins if the value is above 0.02 mm. Compared to Wang et al. [18] where the feed rate has a small effect on the subsurface damage area, a significant difference of the damage area start is detected. Changing the feed from 0.03 to 0.065 mm/tooth means an average increase of 9.5° of the start fibre cutting angle θ_{ne} across all tools. The damage area also starts earlier, changing from 0.065 to 0.1 mm/tooth, but only by an average of 3.6°.

The end of the damage area varies slightly with decreasing chip thickness down to chip thickness of 0.02 mm. Considering the standard deviation all ends remain almost the same for all tools at chip thicknesses above 0.02 mm. Here the deviation from minimum to maximum fibre cutting angle θ_{ne} value is highest at the tool T1 with 6°. The smallest deviation in the end value is 1.6° for tool T5, the tool with the smallest rake angle, see Fig. 7e. This tool also shows the latest end of the damage area with an average value of $\theta_{ne} = 28.7°$. The earliest end is on tool T2 with a value of 36.3°. Chip thickness values below 0.02 mm show the same trend for all milling cutters as T3 at the begin of the damage area. The θ_{ne} values increase again, indicating an earlier end.

4.2.2. Influence of the tool on damage area

There is an influence of the tool rake angle on the area of surface cavities. The damage area starts earlier with a larger rake angle. Due to the rake angle, the cutting edge hits the fibre at a different effective cutting angle. If the defined cutting angle θ_{ne} is corrected by the normal rake angle γ_{ne} by subtracting it (Fig. 3b), it can be seen that the bending of the fibre starts at almost the same local condition. At a feed rate of 0.065 mm/tooth the angle deviation between the tools can be reduced from 12° to 13° (Fig. 8) to 2 and 1°. For example, the observed angle of 82.9° for T3 is corrected by $\gamma_{ne} = 22°$ calculated by the simulation to a value of 60.9°. For the tools with rake angles of −7° and 9°, this gives corrected damage start values of 63.1° and 61.8°. Particularly for the helical tools, it can be seen that the θ_{ne} value at the end of the damage

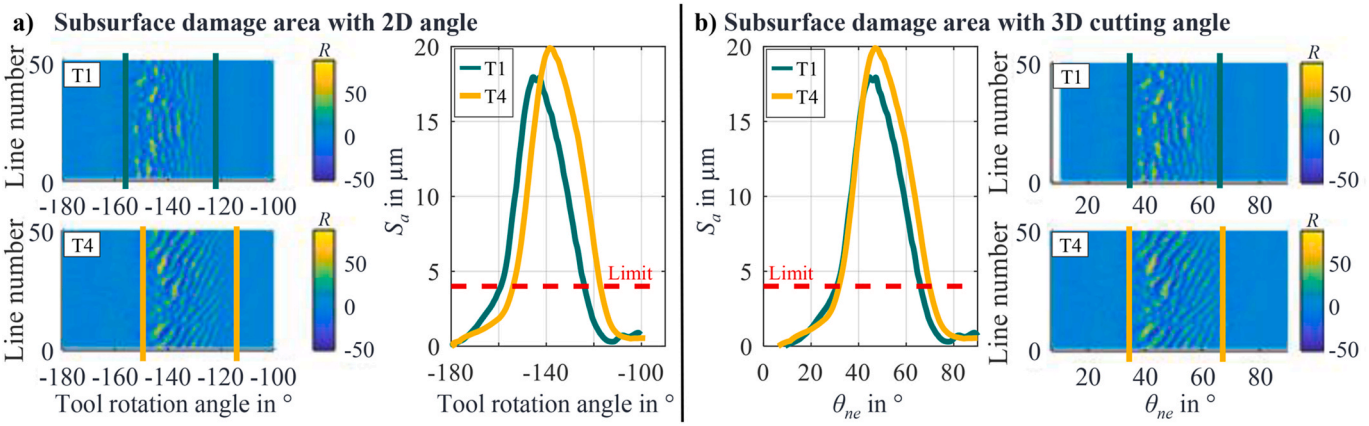

Fig. 6. Influence of the 3D cutting angle by comparison of T1 ($\lambda = 0°$ and $\gamma = 8°$) with T4 ($\lambda = 30°$ and $\gamma = 9°$), $\Phi = 80°$and $f_z = 0.065$ mm/tooth.

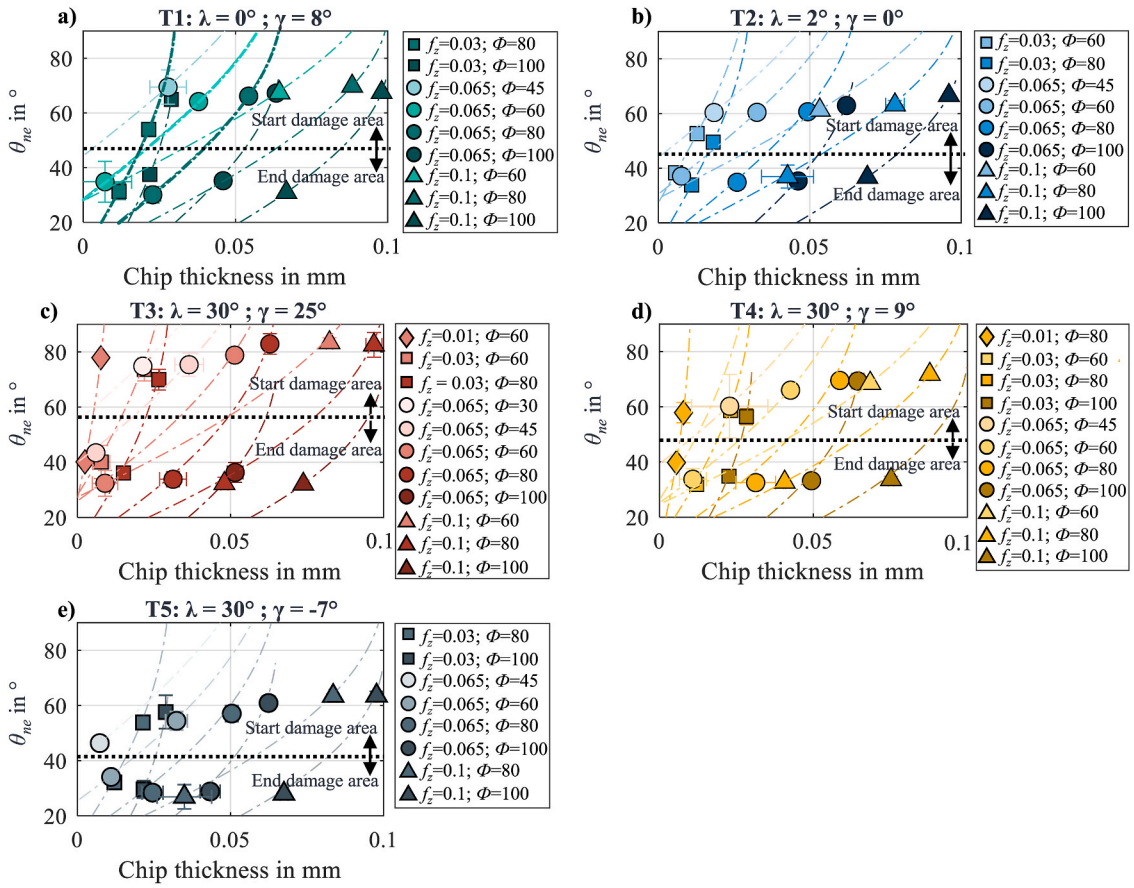

Fig. 7. Detected damage areas for all tools due to different fibre orientations and feed rates.

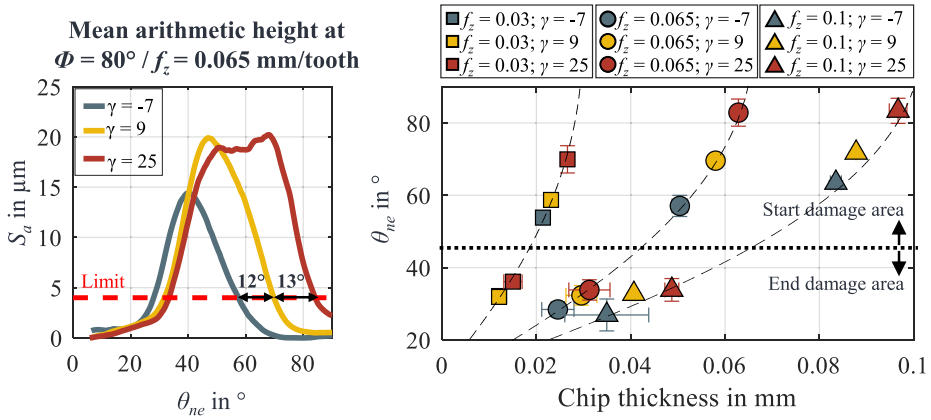

Fig. 8. Influence of the rake angle (comparing tools with helix angle).

area tends to increase with the rake angle, i.e. an earlier end. The trend is smaller compared to the start. This results in a larger damage area at higher rake angle. The lower influence at the end can be explained by the increasing proportion of cutting edge rounding with decreasing chip thickness across the cut. This means that the effects of the rake angle on the cutting mechanism decrease over the cut, while the significance of the cutting edge rounding increases. The cutting edge rounding is crucial for achieving the bending strength and the subsequent shearing, especially with small chip thicknesses. As mentioned before, a chip thickness of 0.02, a clear increase in θ_{ne} at the end can be observed for all milling tools. The cutting edge rounding and thus the effective rake angle, which assumes a high negative value at this point, prevents the bending of the fibres and thus the occurrence of surface cavities. It can be assumed that the cutting edge rounding has also a significant influence at the beginning of damage area at lower chip thicknesses. This can be seen from the significantly smaller effect of the chip thickness on the start and end of the cutting angle for chip thickness lower 0.03 mm. It can be inferred from the data that the effect of cutting edge rounding to the damage area differs from starting the engagement with the rake angle to cut with the cutting edge rounding over the entire cut.

4.3. *Characteristics and formation mechanism of subsurface damage area*

4.3.1. *Influence of fibre orientation on damage depth*

The damage depth in the detected subsurface damage area (SDA) varies within one cut due to different combinations of fibre cutting

angles θ_{ne} and chip thickness. This is shown in Fig. 9 as an example for tool T1, the one without helix angle, for fibre orientations 60, 80 and 100°. The surface roughness shows that at high θ_{ne} the damage structure is initially less wide and deep in the subsurface damage area. This represents the deviation from the ideal cutting contour and thus the shape of the saw teeth. This means initially the subsurface damage area starts with smaller saw teeth. The size of the saw teeth can be correlated with the surface roughness value S_z, which indicates the maximum level of damage depth for each fibre cutting angle θ_{ne}. The S_z values in Fig. 9 show that if the structure on the surface roughness the damage depth initially increases, although the chip thickness decreases. This is the opposite trend found by Voβ [17] where greater chip thickness results in larger saw tooth profiles. The differing finding can be explained by the changing fibre cutting angle θ_{ne} during one milling cut. In addition to the chip thickness, θ_{ne} affects the damage depth and thus the size of the saw teeth. With a declining θ_{ne} the depth of the saw teeth get larger up to a certain fibre cutting angle, where the damage depth represented by S_z drops, see Fig. 9. This drop is steeper for larger chip thicknesses. The position of the highest S_z varies and is considered in more detail below. Assuming that the interfacial crack due to the fibre bending occurs at the same length for the fibre cutting angles θ_{ne} 40° and 60° helps to understand the influence of θ_{ne}, see Fig. 10a. Since the depth of the saw tooth is orthogonal to the tangent of the circular path on which the tool runs, the angle between the saw tooth depth and the length of the interlaminar crack (l_{ic}) is the same as the fibre cutting angle. This means that the length of depth (l_d) can be calculated by $\cos(\theta_{ne}) \bullet l_{ic}$. Since the cos(60°) is less than cos(40°) the theoretical damage depth higher at θ_{ne} = 40°. In addition, a larger θ_{ne} means that a greater distance has to be travelled for the same bending moment. This means that the fibre has already bent further for the same distance. Conversely, a higher bending moment is applied after a shorter distance due to larger θ_{ne} values and therefore the bending strength is exceeded earlier.

4.3.2. *Real cutting conditions and influence on process forces*

If comparing the theoretical uncut chip thickness with the maximum damage depth S_z it comes apparent that even for the lower damage depths the cavities are mostly deeper than the chip thickness, see Fig. 10b. In the identified subsurface damage area, this means that the damage depth over the tool height exceeds the chip thickness at least at one point after a certain fibre cutting angle θ_{ne}. In the experiments in Fig. 10 it is about θ_{ne} = 60°. For high feed rates of 0.1 mm/tooth S_z can be up to three times higher. This means that the cutting edge hits already damaged surface with every tool rotation and therefore does not always hit material over the entire height of the tool, see Fig. 10b.The fact that material is not permanently in contact with the cutting edge is recognized in the evaluation of the forces. Fig. 11 shows the forces during one cut in down-milling for a twisted tool. From a global perspective the entry of the first cutting edge point in the subsurface damage area ($S_{first,start}$) leads to decreasing parallel and transverse forces in the laminate plane. This can be explained by the lack of material due to the saw teeth and the crack initiation of the interlaminar fracture due to the fibre bending. The forces are minimum as long as the tool is in contact with the damage area with almost the entire tool height and start to increase when the first cutting edge point exits the damage area ($S_{first,end}$). When the first cutting edge point enters the subsurface damage area local increases followed by a drop of the forces can be observed, see Fig. 11. This occurs in all three force directions and the local peaks are repeated until the last cutting edge point emerges from the damage area ($S_{last,end}$). The local force peaks can be explained by the impact of the hitting the existing saw tooth profile as shown in Fig. 10b. The contact of the cutting edge on a saw tooth thus leads to a brief increase in force, which is followed by a drop as the resistance to the cutting edge decrease due to the interlaminar fracture. This is followed by another increase when the shear-induced fibre fractures occur and the next contact takes places. Before the first entry into the damage area the signal is smooth. After the last cutting edge point emerges from the damage area, peaks are still present, but much smaller. This can be explained by the excitation of the frequency by the impact on the saw teeth.

Fig. 12 shows a force signal with a greater depth of damage. Here it becomes clear that the individual milling cuts differ from each other. A peak due to the impact on the saw tooth is followed by a dip in the subsequent cut, as a surface cavity has formed here. This is then followed by another peak in the third cut. This clearly shows how the formation of the saw tooth profile is mapped via the force signals. With increasing cutting edge rounding, a decrease in the peaks can be observed and a more uniform signal is produced across different cuts.

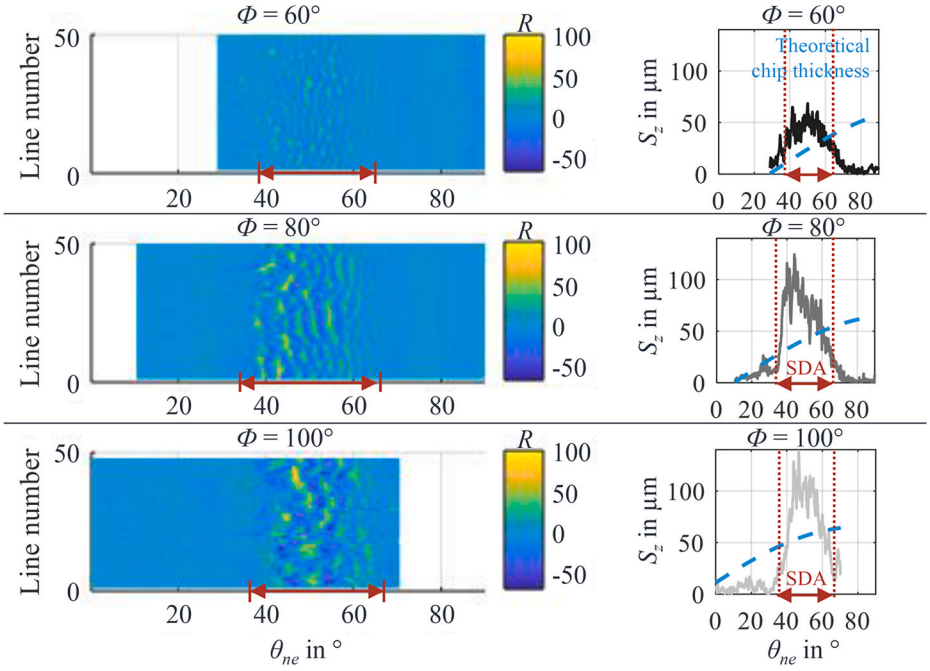

Fig. 9. Surface roughness and resulting S_z for fibre orientations 60°, 80° and 100° with T1 (λ = 0° and γ = 8°) and f_z = 0.065 mm/tooth.

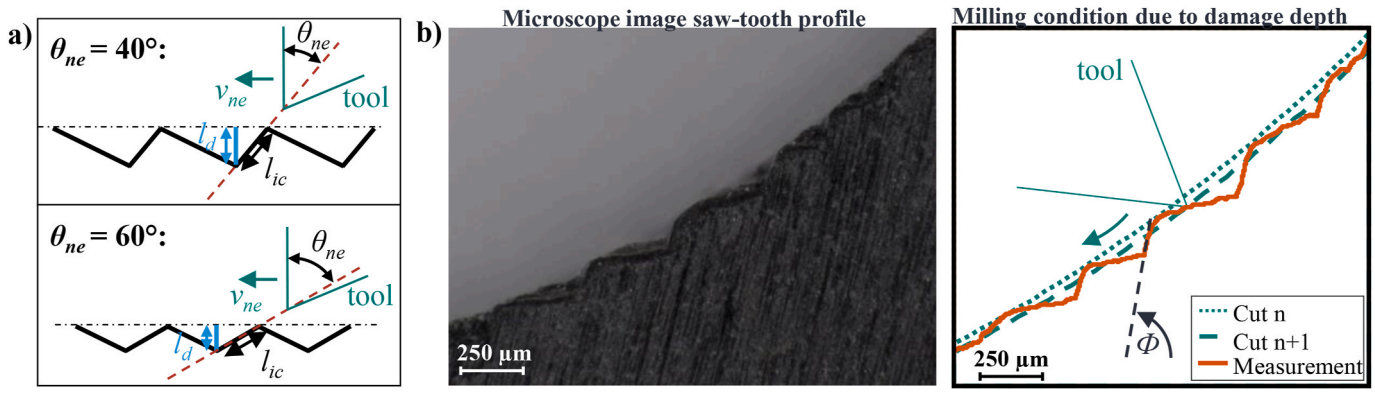

Fig. 10. Saw teeth profile in a) schematically shown for different θ_{ne} and in b) real saw teeth over one cut and the illustration of resulting milling condition due to theoretical uncut chip thickness.

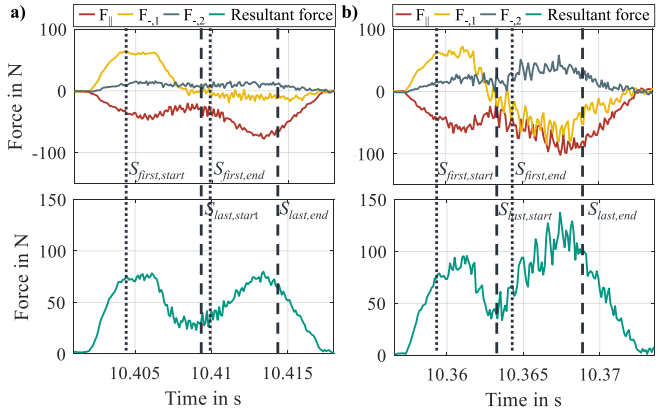

Fig. 11. Comparison of forces across one cut for a) feed rate of 0.03 mm/tooth and b) feed rate of 0.065 mm/tooth with tool T3 ($\lambda = 30°$ and $\gamma = 25°$).

4.3.3. *Influence of tool and chip thickness on damage depth*

The effect of chip thickness on the damage depth can be analysed by comparing the same fibre orientation with different feed per tooth. The fibre cutting angles θ_{ne} remain the same while resulting chip thicknesses change. This confirms the effect observed by Voß [17] that the saw tooth profile becomes smaller as the chip thickness decreases. So the damage depth is less with a lower feed per tooth. This can be seen for S_z from the surface measurement (Fig. 9), but it can also by comparing the force signals over one cut (Fig. 11). The intervals between the local force peaks increase in height and width at higher feed rates, which can be explained by the deeper damage and thus larger saw teeth. Both the longer cantilever and the force generated by the greater localised chip thickness lead to higher bending moments, resulting in deeper interlaminar cracks represented by the localised force reduction.

All experiments plotted against chip thickness (Fig. 13a) show that the decreasing trend in maximum damage depth due to decreasing chip thickness applies to most experiments. However, chip thickness below 0.01 mm leads to increased damage depth. Due to the effect that the chip thickness is constantly below the cutting edge rounding there will be another effective rake angle in material contact. Up to 0.01 mm the smaller the chip thickness, the smaller the maximum damage. As with the detection of damaged areas, the trend reverses after this value and increases again with greater gradient. As mentioned before the position of the maximum damage depth S_z varies due to the uncut chip thickness, see Fig. 13b. For each feed per tooth the fibre cutting angle θ_{ne} of maximum S_z decreases with decreasing chip thickness. The higher the feed rate, the more pronounced the phenomenon that the highest damage value changes its position. This can be explained by the significance of the fibre cutting angle influence on the depth of damage increases with greater chip thicknesses, see Fig. 11a.

The rake angle also influences the depth of damage. It can be seen in Fig. 13c that with a smaller rake angle, the deepest damage is located at smaller cutting angles. However, this only applies when comparing the helical tools. Because the position of the deepest damage shifts with both rake angle and chip thickness, different results occur when the influence of the rake angle on the damage depth is recorded. At lower fibre cutting angles θ_{ne} lower rake angles lead to deeper damage, while at higher fibre cutting angles θ_{ne} increased rake angles lead to deeper damage. Especially for T3 with the large positive rake angle of 25°, the damage depth at the damage area start is particularly high. The rake angle and the greater chip thickness at cutting angles around 60–70° create a lever effect that causes deep damage.

The micro-geometry of the cutting edge influences the damage depth. This can be seen by comparing the same test points with different edge rounding (Fig. 14). There is a cutting edge rounding at which the

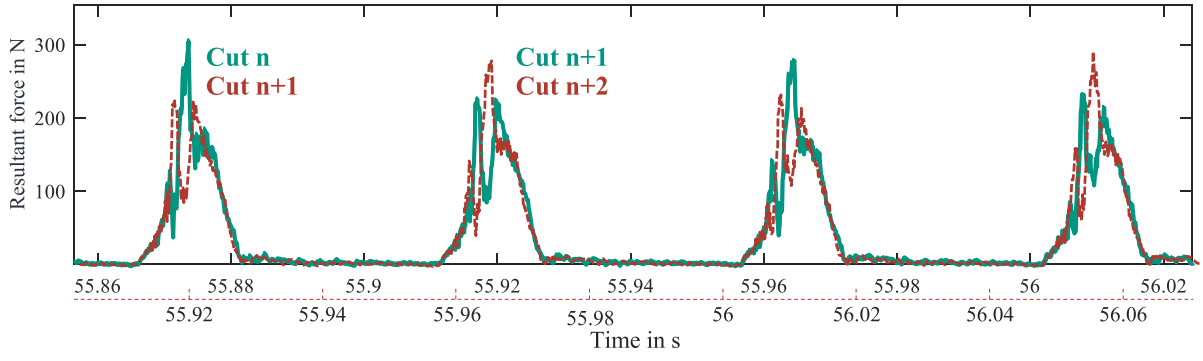

Fig. 12. Force amount over four cuts superimposed with the following cut (T3: $\lambda = 30°$ and $\gamma = 25°$; $f_z = 0.065$; $\Phi = 100°$).

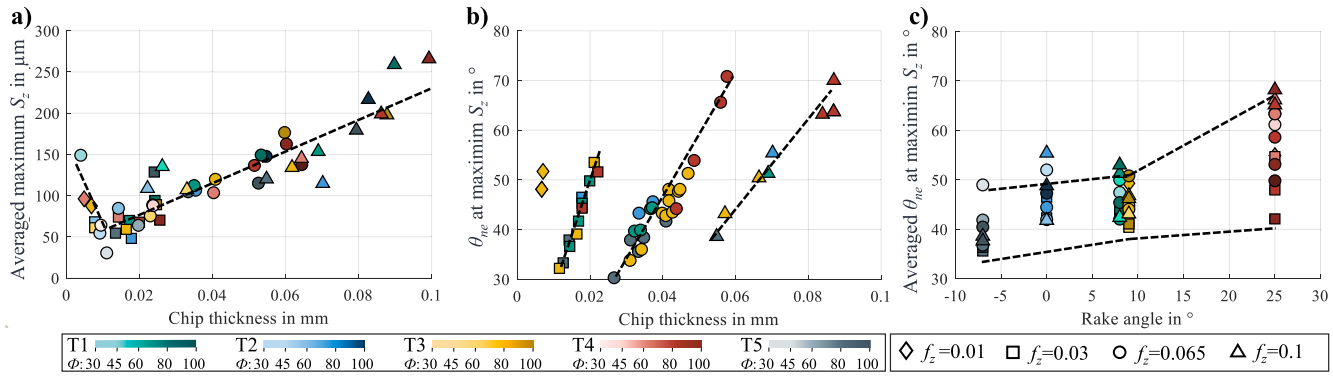

Fig. 13. Damage depth of surface cavities a) Averaged maximum S_z for all experiments b) θ_{ne} at maximum S_z at $\Phi = 80°$ c) Averaged θ_{ne} at maximum S_z for all experiments.

damage is minimal. That does not correspond to the sharpest cutting edge condition and contradicts the statement often made in the literature that a sharp edge leads to less damage during machining. In fact, many experiments show that the quality initially improves with increasing rounding, but further rounding leads to a damage depth that is deeper than that with the smallest cutting edge rounding (Fig. 14). This can be observed by smaller local force peaks with medium cutting edge rounding.

4.3.4. *Effects of damage depth during the cut on the resulting final surface*

In some tests, the initially sharp cutting edge leads to an interfacial crack that reaches up to 2.5 cm in depth, resulting in the destruction of the entire specimen, see Fig. 15. This deep interfacial cracks can be detected in the force signal. In a view across all cuts sudden peaks can be seen. These were also observed by Wang et al. [18] in the area of the surface cavities. If these peaks are viewed across one cut, an extension of the actual cut duration is detected. Initially, the forces decrease, which explains the bending or in this case the splitting of the sample. Then there is a sudden increase in force parallel and transverse to the fibre orientation. This can be explained by more split-off material than by the usual separation mechanism. Then the material is sheared off by the shear induced fibre breaks. In the same test with a more rounded cutting edge ($r_\beta = 13$ µm) the peaks in the force signal can also be observed. However, at first glance no deep interfacial cracks can be seen. Examining the sample in a CT-Scan with cross section along the feed direction, surface cavities much deeper than the usually detected appear (see resulting surface in the middle of Fig. 15). The cross section of the CT-Scan along feed direction lays 0.02 mm away from the edge of the specimen. The sudden peaks in the force signal are therefore an indication of deeper damage in the subsurface damage area. The same test with a rounded cutting edge of $r_\beta = 18$ µm leads to force signals nearly without sudden peaks and thus to an intact surface. It can therefore be observed that here the initially sharp cutting edge produces poorer qualities.

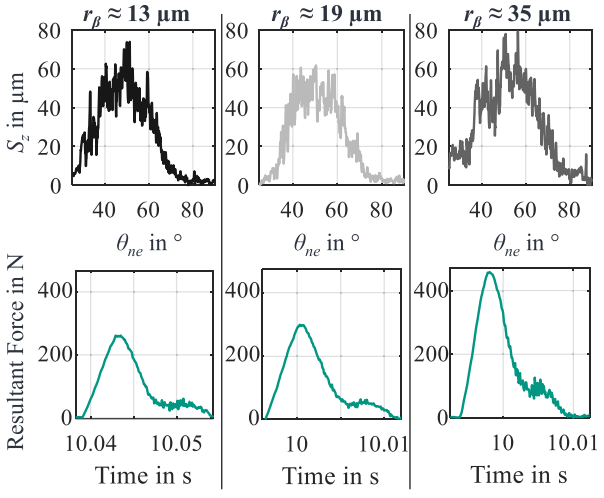

Fig. 14. Maximum height a force amount due to different cutting edge rounding for experiment with T4, $\Phi = 60°$ and $f_z = 0.065$ mm/tooth.

The depth of damage is also particularly significant if the damage area occurs close to the cutting edge exit. It can be seen that the damage depth at the detected end can affect the final resulting surface. Fig. 16 shows the effect of the damage depth in the identified damage area on the final surface at different feed rates. Although the end of the damage area is detected at a feed rate of 0.065 mm/tooth before θ_{ne} on the final resulting surface (Fig. 5), individual damaged points are visible. A pattern is created that no longer corresponds to the saw-tooth profile. It comes apparent that the mechanism of bending and sharing is no longer effective. This phenomenon occurs when the S_z within the damage area reaches so deep that the final surface is damaged through as it reaches deeper than the next cut. The depth within the subsurface damage area therefore correlates with the pattern appearing on the surface. A lower damage depth results in less and less deep damage, while higher a S_z significantly affects the damage of the final surface.

4.4. *Milling of an external radius*

In order to evaluate the effects of the findings on the actual resulting surfaces during a milling process of a curved surface, tests were carried out in up and down milling. An outer radius with 6 mm is milled with T2, feed rate of 0.065 mm/tooth and thus a changing fibre cutting angle θ_{ne} at the last cutting edge contact (from $\theta_{ne} = 80°$ to $\theta_{ne} = -10$) is examined, see Fig. 17a.

Fig. 17b shows that the damage area ends earlier in the up-milling than in the down-milling, if the start damage value is defined as the higher and the end as the lower θ_{ne}. The earlier end at $\theta_{ne} = 48°$ can be explained by the entry at minimum chip thickness in up-milling. In particular, the detected increase for the end value in the evaluation over one cut in down-milling at chip thicknesses smaller than 0.02 mm explains the earlier end. The damage area in down-milling ends at an earlier value of around $\theta_{ne} = 26°$. This can be explained by the damage depth caused within the cut extends to the resulting surface. The higher θ_{ne} start value in the up-milling process can also be explained by deeper damage in the following cut. An additional effect of up-milling is that the damage at the start extends even further into the surface that is otherwise undamaged surface. One possible explanation for this is that the cutting edge hits an already damaged surface and the mechanism of action of bending away is thus extended even further. Gradually, however, the damage reaches less deeply, the fibres therefore do no longer bend and the phenomenon disappears. The range of surface cavities

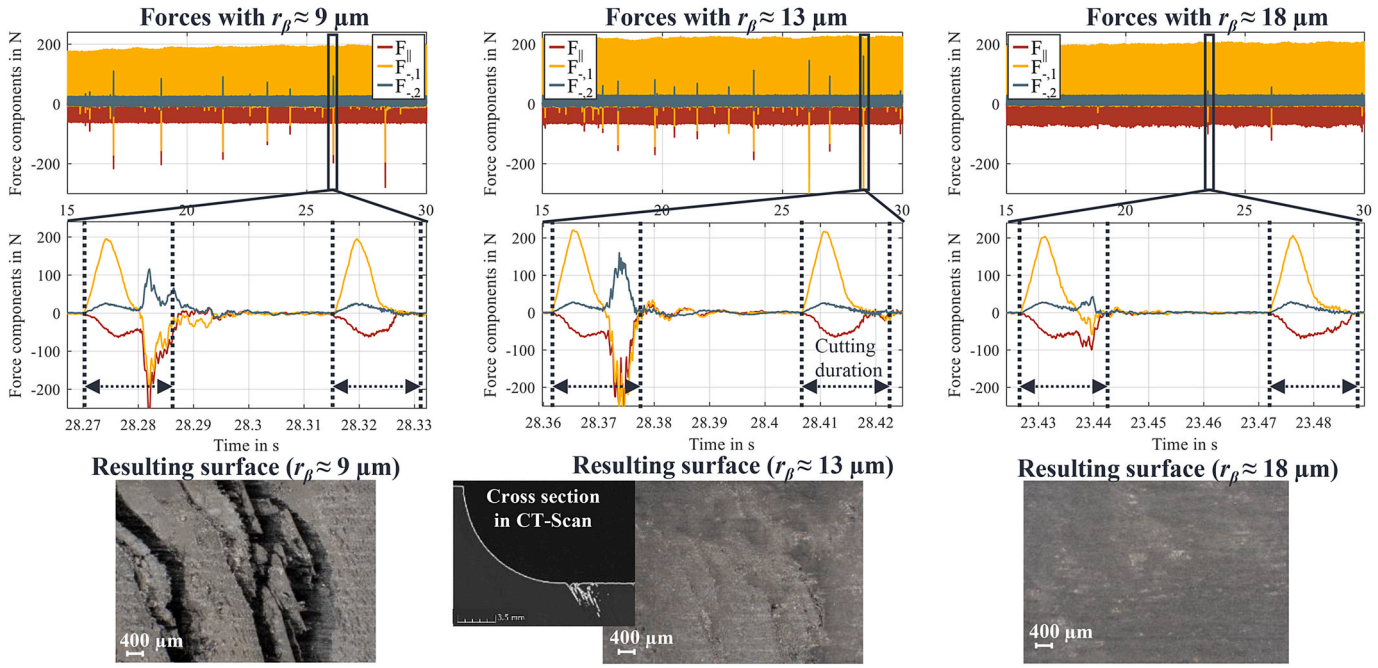

Fig. 15. Influence cutting edge rounding on forces and surface quality with $\Phi = 60°$ and $f_z = 0.03$ mm/tooth.

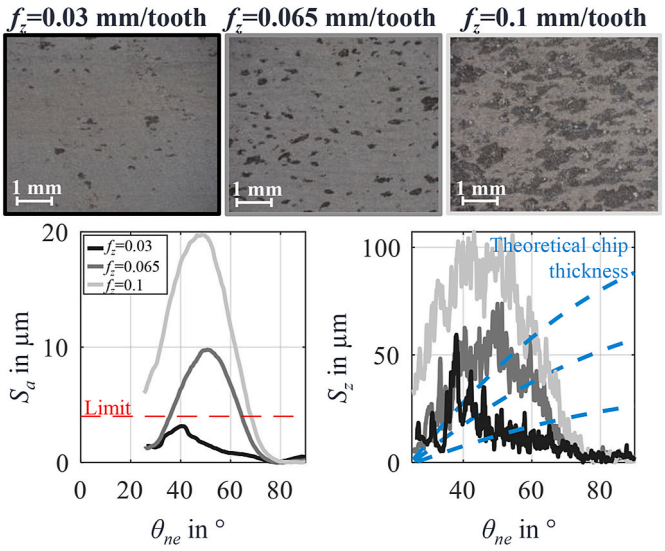

Fig. 16. Influence damage area and damage depth on the final resulting surface (end of the cut) in the test with T4 and $\Phi = 60°$.

could be minimised if the external radius from $\theta_{ne} = -10°$ to $\theta_{ne} = 60°$ (the intersection of the up- and down-milled S_a curves) is milled in up-milling, while the range from $\theta_{ne} = 80°$ to $\theta_{ne} = 60°$ will be machined in down-milling.

5. Conclusion

Extensive peripheral milling test were carried out on UD-CFRP with five different tool geometries and evaluated based on simulation using the spatial fibre cutting angle $\theta_{ne,}$ defined in the effective normal plane. The new experimental setup with the associated analysis over one milling cut provide deep insights into the formation mechanism and influencing factors of the subsurface damage area.

- The area with saw tooth formation depends in particular on the tool geometry and the chip thickness.
  - o The rake angle has a major influence on the start of the damage area and the larger it is, the earlier the area begins. For moderate rake angles $\gamma = 0$–$9°$, the saw tooth profile is formed in a maximum range of 30°–70° θ_{ne}. At $\gamma = 25°$ the range is $\theta_{ne} = 30°$ to $\theta_{ne} = 85°$ and at $\gamma = -7°$ from $\theta_{ne} = 25°$ to $\theta_{ne} = 65°$.
  - o The influence of the chip thickness is smaller in comparison, but can be seen in both the start and end of the damage area. The trends change in particular with chip thickness below 0.02 mm. The cutting edge rounding due to the effective rake angle comes increasingly into material contact. This leads to an earlier end of the damage area.
- The depth of damage and the form of the saw teeth depends on the chip thickness, rake angle, cutting edge rounding but additionally the fibre cutting angle has an influence. The maximum damage depth decreases over declining chip thickness. After a minimum of 0.01 mm, the damage increases again. The position of maximum damage shifts due to chip thickness and rake angle.
- The saw-tooth profile results in temporary loss of contact between tool and material. This can be recorded by local force peaks. The peak height and width correlates with saw tooth size. A moderate cutting edge rounding of about 15–25 µm showed the lowest damage values. Initially sharp cutting edges can lead to deep interlaminar cracks and to a total failure of the specimen. Detectable by high force peaks and an extension of the theoretical cutting time.
- The milling of an external radius shows that understanding what happens during the cut and how the parameters affect the damage area is important for the damage on the final resulting surface. The damage depth in the subsurface damage area is important as it can still affect the resulting surface, even though the damage area ends earlier. The identified subsurface damage range at of 44–65 % of the entire 90° range at which the fibre is inclined to the cutting edge is extended up to 12 %. The decisive factor for the direction of the damage expansion is whether up or down milling is used.

A precise knowledge of the damage areas and parameters influencing the damage makes it possible to avoid this area or minimise the damage depth by adapting the parameters appropriately due to θ_{ne}. The

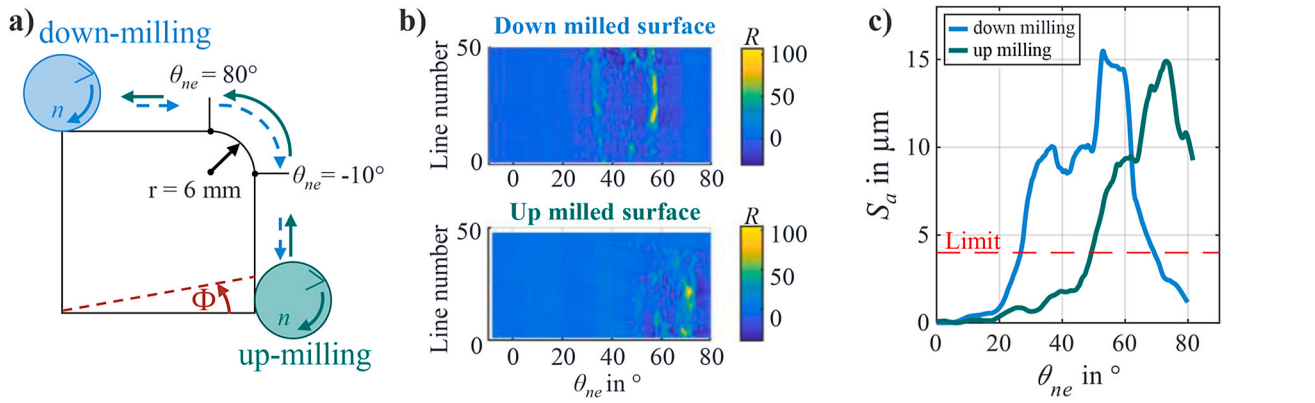

Fig. 17. Milling an external radius a) schematic milling path, b) surface roughness of up and down milling in the external radius and c) S_a in up and down milling of the external radius.

simulative spatial evaluation can be used to investigate complex tool geometries and process paths such as wobble milling. In addition, the application to different matrix-fibre combination must be investigated, as the material properties in particular are decisive for the cutting mechanism of saw-tooth formation.

CRediT authorship contribution statement

Felicitas Böhland: Writing – original draft, Visualization, Validation, Software, Methodology, Investigation, Formal analysis, Conceptualization. **Andreas Hilligardt:** Writing – review & editing, Supervision, Software. **Volker Schulze:** Writing – review & editing, Supervision, Funding acquisition.

Declaration of competing interest

The authors declare that they have no known competing financial interests or personal relationships that could have appeared to influence the work reported in this paper.

Data availability

Data will be made available on request.

Acknowledgement

The authors acknowledge gratefully the funding support of the German Research Foundation (DFG) within the International Research Training Group “Integrated engineering of continuous discontinuous long fiber reinforced polymer structures” (IRTG 2078).

References

[1] Schürmann H. Konstuieren mit Faser-Kunststoff-Verbunden. Berlin, Heidelberg: Springer; 2007.
[2] Ehrenstein GW. Faserverbund-kunststoffe. Werkstoffe – verarbeitung – eigenschaften. München: Hanser; 2006.
[3] Rummenhöller S. Werkstofforientierte Prozeßauslegung für das Fräsen kohlenstofffaserstärkte Kunststoffe, TH. Dissertation: Aachen; 1996.
[4] Colligan K, Ramulu M. Delamination in surface plies of graphite/epoxy caused by the edge trimming process. In: Processing and manufacturing of composite materials; 1991. p. 27.
[5] Hocheng H, Puw H, Huang Y. Preliminary study on milling of unidirectional carbon fibre reinforced plastics. Compos Manuf 1993;4:103–8.
[6] Haddad M, Zitoune R, Bougherara H, Eyma F, Castanié B. Study of trimming damages of CFRP structures in function of the machining processes and their impact on the mechanical behavior. Composites Part B 2014;57:136–43.
[7] Schütte C. Bohren und Hobeln von kohlenstofffaserverstärkten Kunststoffen unter besonderer Berücksichtigung der Schneide-Faser-Lage. Hamburg, TU: Dissertation; 2014.
[8] Hohensee V. Umrissbearbeitung faserverstärkter Kunststoffe durch Fräsen und Laserschneiden. Dissertation: Hannover Univ.; 1992.
[9] Hintze W, Brügmann F. Influence of spatial tool inclination on delamination when milling CFRP. J Mater Process Technol 2018;252:830–7.
[10] Zhang B, Li Y, Wang F, Yang L, Deng J, Lin Y, He Q. Machining inclination selection method for surface milling of CFRP workpieces with low cutting induced damage. Compos Struct 2023;304:116585.
[11] Seeholzer L, Scheuner D, Wegener K. Analytical force model for drilling out unidirectional carbon fibre reinforced polymers (CFRP). J Mater Process Technol 2020;278:116489.
[12] Hintze W, Hartmann D, Schütte C. Occurrence and propagation of delamination during the machining of carbon fibre reinforced (CFRPs) – an experimental study. Compos Sci Technol 2011;71:1719–26.
[13] Kindler J. Werkstückqualität und Standzeitoptimierung von Zerspanwerkzeugen bei der Unrissbearbeitung von kohlenstofffaserverstärkten Kunststoffen. Hamburg, TU: Dissertation; 2010.
[14] Wang XM, Zhang LC. An experimental investigation into the orthogonal cutting of unidirectional fibre reinforced plastics. Int J Mach Tool Manufact 2003;43:1015–22.
[15] Sheikh-Ahmad JY. Machining of polymer composites. New York, London: Springer; 2009.
[16] Henerichs M, Voß R, Kuster F, Wegener K. Machining of carbon fiber reinforced plastics: influence of tool geometry and fiber orientation. CIRP Journal of Manufacturing Science and Technology 2015;9:136–45.
[17] Voß R. Fundamentals of carbon fibre reinforced polymer (CFRP) machining. Zuerich: Dissertation; 2017. ETH.
[18] Wang C, Liu G, An Q, Chen M. Occurrence and formation mechanism of surface cavity defects during orthogonal milling of CFRP. Compos B Eng 2017;109:10–22.
[19] Liu C, Ren J, Shi K, Zhang Y. Investigation of fracture mechanism evolution model for UD-CFRP and MD-CFRP during the milling process. Compos Struct 2023;306:116585.
[20] Jahromi AS, Bahr B, Krishnan KK. An analytical method for predicting damage zone in orthogonal machining of unidirectional composites. J Compos Mater 2014;48(27):3355e65.
[21] Calzada KA, Kapoor SG, DeVor RE, Samuel J, Srivastava AK. Modeling and interpretation of fiber orientation-based failure mechanisms in machining of carbon fiber-reinforced polymer composites. J Manuf Process 2012;14(2):141e9.
[22] Sauer K, Witt M, Putz M. Influence of cutting edge radius on process forces in orthogonal machining of carbon fibre reinforced plastics (CFRP). Procedia CIRP 2019:218–23.
[23] Wang F, Yin J, Ma J, Jia Z, Yang F, Niu B. Effects of cutting edge radius and fiber cutting angle on the cutting-induced surface damage in machining of unidirectional CFRP composite laminates. Int J Adv Manuf Technol 2017;91:3107–20.
[24] Peter M, Sauer K, Regel J, Dix M. Effects of orthogonal cutting with different cutting edge microgeometry on the surface integrity of unidirectional carbon fibre reinfored plastics. In: MIC procedia; 2022. p. 80–7.
[25] Clemens R, Barth E, Uhlmann E, Zhan Y, Caylak Il, Mahnken R. Effects on process forces of individual milling tool edges depending on the cutting angle. In: Proceedings of the machining innovations conference for aerospace industry (MIC); 2022.
[26] Freese J de, Holtmannspötter J, Raschendorfer S, Hofmann T. End milling of Carbon Fiber Reinforced Plastics as surface pretreatment for adhesive bonding – effect of interlaminar damages and partile residues. J Adhes 2020;12:1122–40.
[27] Hilligardt A, Böhland F, Klose J, Gerstenmeyer M, Schulze V. A new approach for local cutting force modeling enabling the transfer between different milling conditions and tool geometries. Procedia CIRP 2021;102:138–43.
[28] Montoya M, Calamaz M, Gehin D, Girot F. Evaluation of the performance of coated and uncoated carbide tools in drilling thick CFRP/aluminium alloy stacks. Int J Adv Manuf Technol 2013;68:2111–20.